Characterization methodology for pseudomorphic high electron mobility transistors using surface photovoltage spectroscopy

S. Solodky
Department of Physical Electronics, Faculty of Engineering, Tel Aviv University, Ramat Aviv 69978, Israel

M. Leibovitch
ELTA Electronics Industries Ltd., P.O.B. 330, Ashdod 77102, Israel

N. Ashkenasy
Department of Physical Electronics, Faculty of Engineering, Tel Aviv University, Ramat Aviv 69978, Israel

I. Hallakoun
ELTA Electronics Industries Ltd., P.O.B. 330, Ashdod 77102, Israel

Y. Rosenwaks and Yoram Shapira[a)]
Department of Physical Electronics, Faculty of Engineering, Tel Aviv University, Ramat Aviv 69978, Israel

(Received 5 September 2000; accepted for publication 19 September 2000)

Pseudomorphic high electron mobility transistor structures have been characterized using surface photovoltage spectroscopy and numerical simulations. According to the effect of the electric fields in different regions of the device on the surface photovoltage spectra, a simple empirical model that correlates the spectral parameters and electrical parameters of the structure has been developed. The spectra and their analysis are shown to provide values for the electrical parameters of the structure. The sensitivity of the technique to the device electrical parameters is shown by three different examples. In these examples, the differences in doping level and surface charge have been monitored as well as the nonuniformity of doping level across the wafer. © *2000 American Institute of Physics.* [S0021-8979(00)08324-9]

I. INTRODUCTION

The improved properties of pseudomorphic high electron mobility transistors (PHEMTs) with respect to these of GaAs/AlGaAs high electron mobility transistors have led to intensive integration of the former in the growing market of monolithic microwave integrated circuits. PHEMTs combine the high conductivity of an InGaAs quantum well (QW) layer, which is used as an electron channel, with the properties of wide band gap AlGaAs layers, which make PHEMT very suitable for high power applications.

The complex design and growth procedures of PHEMTs require an efficient characterization technique to provide information on growth quality and device parameters as early in the procedure as possible. The measurement technique should be contactless, nondestructive, fast, and wafer scaled. Indeed, photoluminescence,[1,2] electroreflectance,[3] photoreflectance,[4] x-ray diffraction and reflection,[5] and optical transmission[6] have been used for the characterization of PHEMT structures.

Information about the energy band diagram and related fields and charges is essential for probing the device properties. Surface photovoltage spectroscopy (SPS) is a nondestructive, contactless characterization technique, which seems to fulfill these special requirements because of its great sensitivity to electric fields within the structure. SPS monitors changes in the semiconductor surface work function induced by absorption of monochromatic light in the structure, giving rise to surface photovoltage (SPV). A detailed description of this method and its applications may be found in Ref. 7. Recently, this technique has been successfully applied for the characterization of novel structures and devices such as heterojunction bipolar transistor,[8] multi-QWs,[9] QW lasers,[10] and solar cells.[11]

In this work, PHEMT structures were characterized using SPS measurements and numerical simulations. Section II describes the experimental technique and numerical simulations. In Sec. III the PHEMT SPV spectra obtained experimentally and by numerical simulations are described. The contribution of different regions of the device to the SPV spectrum is revealed and the evolution of the PHEMT SPV spectrum with light intensity is discussed. It is shown that the signal from the QW absorption region changes its sign with decreasing light intensity. This makes it possible to determine the direction of the electric field in the QW. Section IV describes the empirical model that correlates the electrical parameters of the PHEMT structure and spectral parameters. Examples of application of the empirical model for monitoring differences in PHEMT electrical parameters are shown in Sec. V. Deviations in the delta-doping level in different PHEMT structures, differences in surface charge density in structures that underwent different surface treatments, and nonuniformity in delta doping across the wafer are determined. The conclusions are summarized in Sec. VI.

II. SAMPLES AND TOOLS

A PHEMT structure grown by molecular beam epitaxy on a GaAs substrate is shown in Fig. 1. It consists of several

[a)]Author to whom correspondence should be addressed; electronic mail: shapira@eng.tau.ac.il

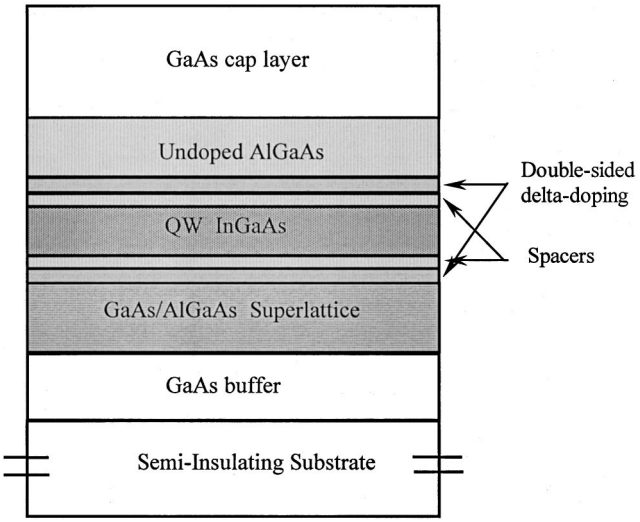

FIG. 1. Typical PHEMT epitaxial structure.

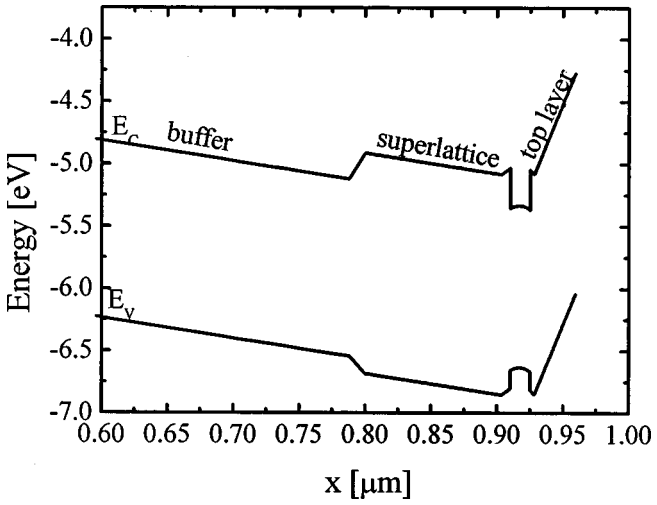

FIG. 2. Equilibrium band diagram of a double-sided delta-doped PHEMT structure.

layers: (1) A wide layer of undoped GaAs buffer is grown on an undoped semi-insulating substrate. The GaAs buffer layer is introduced to prevent substrate defects from reaching the active region of the device. This layer may be composed from different layers including a GaAs/AlGaAs superlattice depending on the manufacturer. (2) Two pulse-doped (delta-doped) layers of $n+$ AlGaAs (with Si sheet concentration in the range of $1-5\times10^{12}$ cm^{-2}) on both sides of the channel are the source of electrons in the conductive channel. (3) Two thin layers of undoped AlGaAs create the spacers that separate the donors further from the channel electrons and reduce Coulomb scattering. (4) An undoped InGaAs QW (with a typical In mole fraction of $\sim$20%) provides the conductive channel where the electrons are strongly confined. (5) An undoped AlGaAs layer (also known as the Schottky layer) on top of the AlGaAs delta-doped layer separates the channel from the gate electrode. (6) The top layer of the structure is a highly doped $n+$ GaAs cap that is used for source and drain ohmic contact formation.

The SPS measurements were performed in air using a commercial Kelvin probe unit (Besocke Delta Phi, Julich, Germany). The optical system consists of 250 W tungsten–halogen lamp, 0.25 m grating monochromator (Oriel) and a set of band pass filters to avoid second order harmonics. The measurement sensitivity is about 1 mV, and the light intensity is on the order of 10 μW/cm^2 at most at a wavelength of 750 nm. Neutral density filters control the light intensity.

The SPV spectra analysis is based on quantitative numerical modeling. The Poisson equation, the continuity equations for electrons and holes, and the current equations are numerically and self-consistently solved.[12] The initial conditions for the numerical model can be obtained from the equilibrium distributions of electrons and holes and the electrostatic potential obtained by the procedure outlined in Ref. 13. Various semiconductor structures based on different materials are present within the device. Therefore, all structure parameters, including electron affinity (work function) and mobility, are considered as position dependent.

The system of the relevant partial differential semiconductor equations, together with appropriate boundary and initial conditions, cannot in general be solved explicitly. Therefore, the solution is calculated numerically. For the specific problem in this work, we use the finite difference method described elsewhere.[14] It has been successfully used for the characterization of different structures and devices. A detailed description of these applications is outlined in Refs. 8–11.

III. RESULTS AND DISCUSSION

Figure 2 shows the calculated equilibrium band diagram of the PHEMT structure (without cap layer). The electric field distribution within the PHEMT epistructure in equilibrium is affected by the doping levels in the delta-doped and cap layers, as well as by interface and surface charges. Carrier redistribution within the entire structure determines the device potential distribution, with nonzero electric fields in the buffer, surface, and QW regions. The buffer/substrate interface (which is at $x=0$) is designed such that the resultant electric field in the buffer layer F_B is high enough to provide good confinement for the electrons, which are driven by the electric field in the channel under operating conditions. The typical value of the potential drop in the buffer layer is usually of about 1 V ($F_B\sim15$ kV/cm). Such a structure is achieved by a special surface treatment of the bare substrate before the growth process.[15]

The field in the top layer F_{top} is very sensitive to the conditions at the external surface and the voltage drop across the Schottky layer may reach 0.7–0.8 eV ($F_{\text{top}}\sim400$ kV/cm) in an actual device. Thus, while electrons are confined in the QW region, holes that escape from it drift further away. Therefore, the electron–hole pairs generated by illumination are separated forming photovoltage (PV) across the structure. Since the directions of the F_B and F_{top} fields are opposite, the PVs resulting from these regions are of an opposite sign.

Figure 3 shows the experimental SPV spectrum of the studied PHEMT structure. At the energy part of the spectrum below 1.41 eV most of the absorption takes place in the

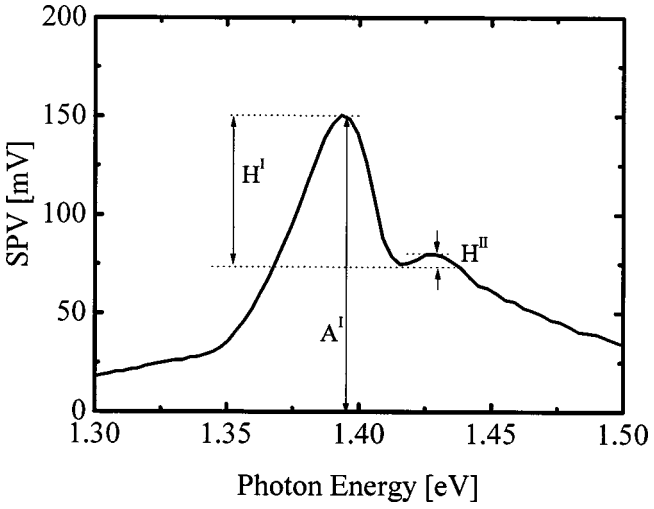

FIG. 3. Typical surface photovoltage spectrum of the studied structure. Labels in the figure correspond to spectrum parametrization scheme.

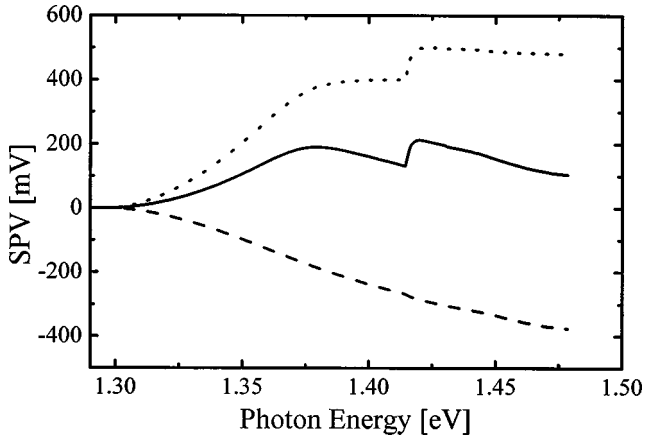

FIG. 4. Calculated photovoltage signal from buffer (dotted curve) and top layers (dashed curve) as a function of photon energy and the resultant SPV spectrum (solid curve).

InGaAs QW. At this portion of the spectrum the SPV moderately increases from a photon energy of 1.3 eV, followed by a sharp peak with a maximum at 1.39 eV. Above 1.41 eV the GaAs buffer and cap layers start to absorb. At this energy range a second wider peak is observed with a maximum at 1.43 eV. Following that peak, the SPV decreases monotonically. Note that absorption at the AlGaAs, which starts at around 1.77 eV (based on the Al mole fraction[16]), is not observed in the spectrum.

At low photon energies, Fermi filling, due to high electron concentration in the channel, dominates the InGaAs absorption coefficient.[17] This effect significantly changes the absorption coefficient of the QW by blueshifting its edge and reducing its magnitude at higher energies. The absorption edge blueshift may be used to yield the electron sheet density in the channel.[3]

The PV magnitude is a complicated function of light absorption, hole escape rate from the well (when absorption takes place in the well), and the electric fields in any given region. To obtain further insight into these processes, numerical calculations described in Sec. II have been performed. The results of such calculations based on the structure studied are shown in Fig. 4, where the SPV spectrum (solid line) together with the separate PV contributions of the buffer (dotted curve) and top layer (dashed curve) are indicated. Indeed, two peaks are observed in the calculated SPV spectrum (solid curve).

In the spectrum region that dominates by absorption in QW the PV from the buffer region increases with photon energy while PV from the top layer region decreases. The signal in this region is a result of hole escape from the QW and redistribution in the buffer/top layer. The sum of these two signals gives the net SPV increase. The signal from the buffer increases until saturation while the signal from the top layer decreases. This leads to the formation of the first peak. The second peak in the SPV is due to the absorption in the GaAs buffer layer, which leads to the appearance of the second step in its PV while the PV from the top layer region continues to decrease. Therefore, the two-peak shape of the spectrum reflects the interplay between the PVs arising from the buffer and top layer fields.

To obtain further insight into the processes that affect the SPV, the evolution of the SPV spectra with light intensity was studied. Figure 5 shows the experimental SPV spectra of the PHEMT structure studied measured at different light intensities. A significant evolution of the spectrum with light intensity is observed. In the low energy region that is dominated by absorption in the QW, a positive SPV slope appears when the light intensity increases from 0.05 to 0.25 μW/cm^2. In the high-energy region corresponding to absorption in GaAs, the slope of the signal changes with increasing light intensity.

At the low energy region of the spectrum, photon absorption and electron hole generation occur primarily in the QW. The PV there is a result of holes escaping from the QW and carrier separation by electric fields. The escape rate of holes from the well depends on the hole barrier height. Depending on the electric field in the QW F_{QW}, the barrier for holes is not equal for the well-buffer V_{buff} and well-top layer V_{top} interface. As a result, the carrier escape rate is also

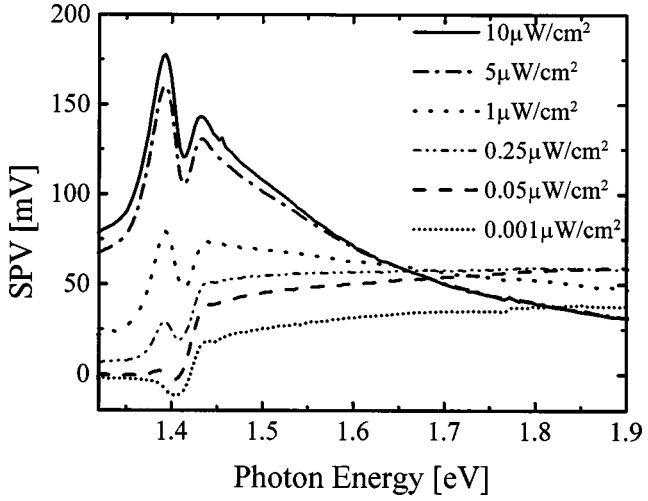

FIG. 5. Surface photovoltage spectra of PHEMT structure measured at different light intensities.

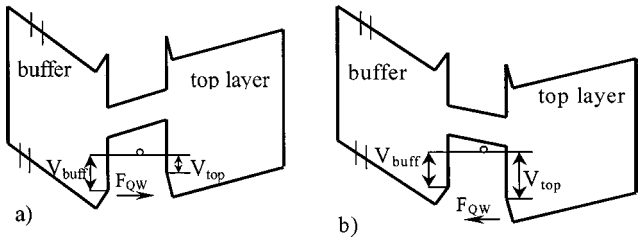

FIG. 6. Schematic representation of the two possible band lineups in the QW region: (a) $V_{top}>V_{buff}$; (b) $V_{buff}>V_{top}$; F_{QW} direction is shown by arrow.

different. This is demonstrated in Fig. 6, where the two possible net F_{QW} directions are schematically shown. Therefore, F_{QW} controls the flow of the photogenerated holes from the QW to the entire structure. The holes induce PV in both the buffer and top layer regions.

At low light intensities, a negative slope of the SPV in the QW region is observed. As explained above, a net negative slope in SPV means that the PV from the top layer region dominates the PV from the buffer region. Hence, the hole escape rate in the top layer direction is higher ($V_{top}<V_{buff}$) than the escape rate in the direction of the buffer layer. This means that the net field direction in the QW is in the same direction as the one in the top layer region [see Fig. 6(a)].

At higher light intensities a positive slope of SPV appears at the QW region. An increase in the light intensity leads to a change in the escape rates from the QW, indicating a change in the sign of F_{QW} under illumination.

IV. EMPIRICAL MODEL

After establishing the relation between the physical mechanisms contributing to PV formation throughout the structure and the ensuing SPV, a simple empirical model has been developed in order to relate spectral features and electrical parameters of the PHEMT structures.

The study described below was performed in order to sort out which PHEMT electrical parameters are most important in defining SPV signal and how they influence the SPV spectrum shape. This was done by a set of numerical simulations. The two-level factorial design[18,19] has been used to define the device structure with different combinations of structural parameters for the present study. In this two-level design the parameter used in simulation gets two values designated by high and low.

The variables for the simulations are the parameters of the PHEMT structure that are expected to have a strong impact on the distribution of electric fields in the PHEMT: top δ_{top} and bottom δ_{bot} delta doping, the surface Q_{sur} and buffer/substrate interface Q_{int} sheet charge densities. The range of the electrical parameters of the structures is $\delta_{top}\subset[3-6\times10^{12}\ \mathrm{cm}^{-2}]$; $\delta_{bot}\subset[0.4-1.5\times10^{12}\ \mathrm{cm}^{-2}]$; $Q_{sur}\subset[0.4-2\times10^{12}\ \mathrm{cm}^{-2}]$, $Q_{int}\subset[0.5-1.6\times10^{12}\ \mathrm{cm}^{-2}]$. The range of the top and bottom delta-doping level corresponds to channel electron sheet density $n_s\subset[1.5-3.5\times10^{12}\ \mathrm{cm}^{-2}]$. This specification of sheet density describes a wide range of current PHEMT device applications (from low noise to high power).

Each range of the electrical parameters was divided into four domains. For each domain the two-level design was performed and an array of 16 (2^4) PHEMT structures was designed. Table I shows the high level and low level values of the parameters chosen for each of the four domains. The low and high levels are designated by *L* and *H*, respectively.

The PHEMT SPV spectrum was parametrized. The parametrization of the spectrum is based on the amplitude of the first peak maximum A^I, and the magnitude of the two peaks with respect to the minimum between them (H^{I} and H^{II}, respectively) (see Fig. 3).

Four simulation sets have been run, each consisting of 16 PHEMT structures. For each run the SPV was calculated from the numerical simulation. The difference in the spectral parameter A^J (relative to a reference structure) is given by

$$\Delta A^J(\delta_{top},\delta_{bot},Q_{sur},Q_{int}) = C_{\delta top}\Delta\delta_{top}+C_{\delta bot}\Delta\delta_{bot}+C_{Qsur}\Delta Q_{sur}+C_{Qint}\Delta Q_{int}, \quad (1)$$

where $C_{\delta top}$, $C_{\delta bot}$, C_{Qsur}, C_{Qint} are coefficients which show the influence of each of the electrical parameter on the spectral parameter A^J. In general, there are additional terms in Eq. (1) that describe the interaction coefficients but in our case these were not found to affect the spectrum. From the data taken from simulations the coefficients $C_{\delta top}$, $C_{\delta bot}$, C_{Qsur}, C_{Qint} were found using the methods described in Refs. 18 and 19. The coefficients are presented in Table II.

The results of our analysis show that the features in the SPV spectrum are closely related to the delta doping levels, and the surface charge density. The height of the second peak H^{II} is practically sensitive only to the bottom delta doping, and shows very weak sensitivity to the other parameters. This is because H^{II} is dominated by absorption in the GaAs buffer layer, and therefore depends only on the electric field in the buffer region F_B. F_B, in return, is greatly affected by the bottom delta doping, and leads to a strong relation between H^{II} and δ_{bot}. H^{I} is affected by the levels of both

TABLE I. Two level values of the structural parameters for four domains of simulations.

Domain No.	$\delta_{top}(\times10^{12}\ \mathrm{cm}^{-2})$		$\delta_{bot}(\times10^{12}\ \mathrm{cm}^{-2})$		$Q_{sur}(\times10^{12}\ \mathrm{cm}^{-2})$		$Q_{int}(\times10^{12}\ \mathrm{cm}^{-2})$	
	L	*H*	*L*	*H*	*L*	*H*	*L*	*H*
1	3	3.6	0.4	0.6	0.4	1.1	0.5	1
2	3.7	4.2	0.7	0.9	0.6	1.3	0.7	1.2
3	4.4	5.1	0.8	1.2	0.8	1.6	0.7	1.4
4	5.3	6	1	1.5	1	2	0.8	1.6

TABLE II. Correlation coefficients between structural parameters and spectral features (shown in Fig. 2).

	$C_{\delta\,\mathrm{top}}$ (mV/10^{12} cm^{-2})	$C_{\delta\,\mathrm{bot}}$ (mV/10^{12} cm^{-2})	$C_{Q\mathrm{surf}}$ (mV/10^{12} cm^{-2})
A^I	130	−295	−175
H^{I}	−10	−95	5
H^{II}	0	125	20

bottom and top delta doping, while the effect of the surface charge density is minor. This is because H^{I} is a result of the strong interplay between the PV from the top and buffer layers. This interplay depends on the electric field distribution in the buffer and top layers, which is defined by the top and bottom delta doping levels. Q_{int} has no pronounced effect on any feature in the spectrum, and therefore cannot be monitored by SPV. This is because the thick buffer layer reduces the effect of Q_{int} on the electric fields in the QW vicinity.

Therefore, taking ΔA^J from the experimental results and substituting it to Eq. (1) makes it possible to evaluate differences in electrical parameters that affect the SPV spectra. The model may be effectively used for determining differences relative to a reference device. In addition, it may be used for monitoring of nonuniformity across a wafer by measuring relative changes in the SPV spectrum from site to site. Such examples will be given in the following sections. It should be emphasized that the presented model is defined for a given light intensity I, but may be successfully applied in wide range of light intensities.

V. SEVERAL APPLICATIONS OF THE EMPIRICAL MODEL

(1) Figure 7 shows the SPV spectra of two different PHEMT structures named PH1 and PH2. The main difference between these structures is a nominal variation of δ_{top} of about 1.5×10^{12} cm^{-2}. Applying the model yields a changes in δ_{top}: $\Delta\delta_{\mathrm{top}}=1.8\times10^{12}$ cm^{-2}. Indeed, the difference in δ_{top} agrees with the nominal value to within 20%,

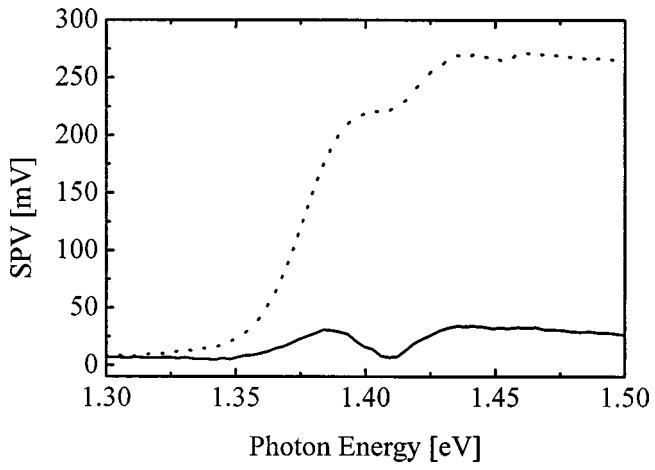

FIG. 7. Surface photovoltage spectra of two PHEMT structures with a difference in effective top delta doping level: (solid curve) PH1 structure; (dotted curve) PH2 structure.

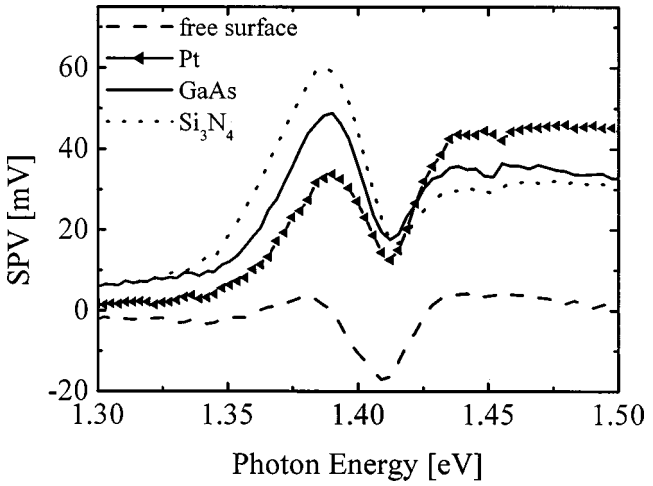

FIG. 8. Surface photovoltage spectra of PHEMT structure with different surface conditions.

which is the estimated relative error. The differences in other parameters are much smaller. Thus, SPS may be successfully applied to monitoring differences in delta-doping density.

(2) As a second example the methodology was applied to monitoring different surface treatments. Samples with different surface conditions have been analyzed. The change of surface conditions changes the charge density at the surface (surface charge) and the electric field at the top layer region. Figure 8 shows SPV spectra of PHEMT structure with AlGaAs free surface, Pt metallization layer, GaAs cap, and Si_3N_4 cap. (The GaAs removal and deposition of Si_3N_4 and a 50 Å thick layer of Pt are important steps in PHEMT technology.) There are significant changes in A^I (relative to the reference sample with GaAs cap). The changes in H^{I} and H^{II} are less significant. The calculated differences in Q_{sur} for each surface treatment (relative to the reference sample) are summarized in Table III. The removal of the GaAs cap causes an increase in surface charge density where as Si_3N_4 and Pt deposition decreases the surface charge density. This illustrates the capability of the methodology to evaluate and compare various surface treatments during device processing and therefore their implication on device performance.

(3) In the last example, the methodology was applied to wafer uniformity monitoring. This was done by recording spectra at different regions across a wafer. In each of the regions the SPV spectra have been measured. A significant nonuniformity in the second peak height (H^{II}) has been observed. Since the changes in H^{II} are strongly affected by the changes in bottom delta-doping density (see Table III), the deviations of the bottom delta doping across the wafer may

TABLE III. Differences in surface charge density calculated for different surface treatments (relative to sample with GaAs cap layer).

	ΔQ_{surf} ($\times10^{12}$ cm^{-2})
GaAs etching	0.3
Si_3N_4 deposition	−0.1
Pt deposition	−0.1

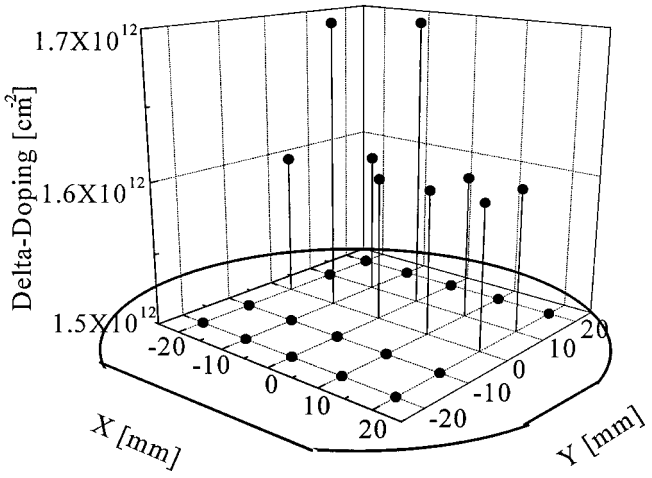

FIG. 9. Values of the bottom delta-doping density in the different regions across the wafer.

be evaluated using Eq. (1). The reference value of delta doping was taken as the value given by the manufacturer: 1.5×10^{12} cm^{-2}. The deviations of bottom delta-doping density from the reference value across the wafer were calculated. Figure 9 shows the values of the bottom delta-doping density in the points on the wafer where the SPV have been measured and the place of the measured points on the wafer relative to the major and minor flats. The calculated deviations from the reference are $\sim 10\%$. This value is in the range of the manufacturer error. Therefore, the SPS technique is sensitive to the nonuniformity in the doping level and may be used as the monitor for the grow quality.

VI. CONCLUSION

A methodology for PHEMT characterization using the SPS technique was developed. The obtained SPV spectra were studied both experimentally and numerically. The calculations make it possible to ''decode'' the contribution of different regions of the device to the SPV spectrum. It was shown that two peaks that appear in all PHEMT SPV spectra originate from the interplay between the PV resulting from the bottom buffer layer and the surface layer of the sample. The PHEMT SPV spectra were found to be sensitive to the light intensity. From this dependence the net electric field direction in the QW region has been determined. The net electric field direction in equilibrium was found to be the same as in the top layer. From numerical simulations a simple empirical model, which correlates spectrum features with PHEMT electrical parameters, was developed. The empirical model was applied for the evaluation of differences in electrical parameters in different PHEMT structures, different surface treatment, and the wafer uniformity characterization. Based on the model, differences in important electrical parameters of PHEMT structures have been extracted: differences in the top delta-doping level of 1.8×10^{12} cm^{-2} between two PHEMT structures (that are in agreement with manufacturer data), differences in surface charge density as a result of different surface treatments, and inhomogeneity in the delta-doping level across a wafer. These three examples demonstrate the ability of the methodology to characterize different process steps and surface treatments as well as wafer growth homogeneity and the sensitivity of the technique to the deviations in the PHEMT electrical parameters.

ACKNOWLEDGMENTS

This research was supported in part by MAFAT and MTI. Y.S. is indebted to Henry and Dina Krongold for their generous support.

[1] M. Wojtowicz, D. Pascua, A. C. Han, T. R. Block, and D. C. Streit, J. Cryst. Growth **175**, 930 (1997).
[2] W. Lu, J. H. Lee, K. Prasad, G.-I. Ng, and P. Lindstrom, J. Phys. D **31**, 159 (1998).
[3] Y. S. Huang, W. D. Sun, L. Malikova, F. H. Pollak, I. Ferguson, H. Hou, Z. C. Feng, T. Ruan, and E. B. Fantner, Appl. Phys. Lett. **74**, 1851 (1999).
[4] D. Y. Lin, S. H. Liang, Y. S. Huang, K. K. Tiong, F. H. Pollak, and K. R. Evans, J. Appl. Phys. **85**, 8235 (1999).
[5] T. J. Rogers, J. M. Ballingall, M. Larsen, and E. L. Hall, J. Vac. Sci. Technol. B **13**, 777 (1995).
[6] D. Y. Lin, Y. S. Huang, K. K. Tiong, F. H. Pollak, and K. R. Evans, Semicond. Sci. Technol. **14**, 103 (1999).
[7] L. Kronik and Y. Shapira, Surf. Sci. Rep. **37**, 1 (1999).
[8] B. Mishori, M. Leibovitch, Y. Shapira, F. H. Pollak, D. C. Streit, and M. Wojtowicz, Appl. Phys. Lett. **73**, 650 (1998).
[9] N. Bachrach-Ashkenasy, L. Kronik, Y. Shapira, Y. Rosenwaks, M. C. Hanna, M. Leibovitch, and P. Ram, Appl. Phys. Lett. **68**, 879 (1996).
[10] N. Ashkenasy, M. Leibovitch, Y. Shapira, F. H. Pollak, T. Burnham, and X. Wang, J. Appl. Phys. **83**, 1146 (1998).
[11] N. Ashkenasy, M. Leibovitch, Y. Rosenwaks, Y. Shapira, K. W. J. Barnham, J. Nelson, and J. Barnes, J. Appl. Phys. **86**, 6902 (1999).
[12] G. A. Ashkinasi, M. G. Leibovitch, and M. Nathan, IEEE Trans. Electron Devices **ED-40**, 285 (1993).
[13] A. Marshak, Solid-State Electron. **24**, 1111 (1981).
[14] S. Seberhorr, *Analysis of Semiconductor Devices* (Springer, New York, 1984).
[15] W. E. Quinn, B. Lauterwasser, J. Kronwasser, T. Mizandi, and D. Carlson, 1997 International Conference of GaAs Manufacturing Technology (MANTEC), pp. 166–168.
[16] F. H. Pollak, in *Properties of Aluminum Gallium Arsenide*, edited by S. Adachi (INSPEC, London, 1993), p. 53.
[17] Y.-H. Zhang and K. Ploog, Phys. Rev. B **45**, 14069 (1992).
[18] H. G. Henry and K. M. Renaldo, 1998 International Conference of GaAs Manufacturing Technology (MANTEC), pp. 195–198.
[19] G. E. P. Box, W. J. Hunter, and J. S. Hunter, *Statistics for Experiments* (Wiley, New York, 1978).